The chain of chirality transfer in tellurium nanocrystals

Ben-moshe, Assaf; Da Silva, Alessandra; Müller, Alexander; Abu-odeh, Anas; Harrison, Patrick; Waelder, Jacob; Niroui, Farnaz; Ophus, Colin; Minor, Andrew M.; Asta, Mark; Theis, Wolfgang; Ercius, Peter; Alivisatos, A. Paul

DOI:
10.1126/science.abf9645

Title: The chain of chirality transfer in tellurium nanocrystals

Authors: Assaf Ben-Moshe[1,2], Alessandra da Silva[3], Alexander Müller[4,5], Anas Abu-Odeh[1,5], Patrick Harrison[3], Jacob Waelder[6]†, Farnaz Niroui[7]†, Colin Ophus[4], Andrew M. Minor[4,5], Mark Asta[1,5], Wolfgang Theis[3], Peter Ercius[4], A. Paul Alivisatos[1,2,8*]

Affiliations:

1. Materials Sciences Division, Ernest Orlando Lawrence Berkeley National Laboratory, Berkeley, CA 94720, USA.
2. Department of Chemistry, University of California, Berkeley, CA 94720, USA.
3. Nanoscale Physics Research Laboratory, School of Physics and Astronomy, University of Birmingham, Edgbaston, Birmingham B15 2TT, UK.
4. National Center for Electron Microscopy, Molecular Foundry, Ernest Orlando Lawrence Berkeley National Laboratory, Berkeley, CA 94720, USA.
5. Department of Materials Science and Engineering, University of California, Berkeley, CA 94720, USA.
6. Department of Physics, University of Washington, Seattle, WA 98195, USA.
7. Miller Research Institute, University of California Berkeley, Berkeley, CA 94720, USA.
8. Kavli Energy NanoScience Institute, Berkeley, CA 94720, USA.

† Current Affiliations: Applied Physics Program, University of Michigan, Ann Arbor, MI 48109, USA (J.W).
Department of Electrical Engineering and Computer Science, Massachusetts Institute of Technology, Cambridge, MA 02139, USA (F.N).
*Corresponding author: paul.alivisatos@berkeley.edu

Abstract: Despite persistent extensive observations of crystals with chiral shapes, the mechanisms underlying their formation are not well-understood. While past studies suggest that chiral shapes can form because of crystallization in the presence of chiral additives, or because of an intrinsic tendency that stems from the crystal structure, there are many cases where these explanations are not suitable or have not been tested. Here, an investigation of model Te nanocrystals provides unique insights into the chain of chirality transfer between crystal structure and shape. We show this transfer is mediated by screw dislocations, and shape chirality is not an outcome of the chiral crystal structure or ligands.

One Sentence Summary: 1. Chirality transfer between crystal structure and shape in model nanocrystals is mediated by screw dislocations

2. The chiral shape of model inorganic nanocrystals arises through a screw dislocation mechanism

Main text: The formation pathway of crystals with chiral shapes has been a topic of controversy (*1*,*2*) for over 170 years, ever since Pasteur (*3*) in 1848 reported the formation of chiral crystals from chiral tartarate molecules. Yet, Pasteur himself only ever obtained achiral shapes of one other chiral molecule, thereby demonstrating that chirality of the crystal structure is not sufficient for the crystal shape to be chiral (*4*). Quartz (*5*,*6*), tellurium (*7*) and mercury sulfide (*8*,*9*) only occasionally form chiral shapes despite their intrinsically chiral crystal structures. For quartz in particular, it is often assumed that chiral shapes stem from the chiral molecular building blocks within the structure (*6*). Further complicating the matter, entirely achiral building blocks or materials with achiral crystal structures sometimes form chirally-shaped crystals (*1*,*2*). Two broad classes of mechanisms for chiral shape formation have been discussed. The first attributes the formation of chiral crystal shapes to differential growth rates of chiral facets. This is possibly mediated by the presence of chiral ligands (*2*,*9*-*11*), but could also result from an intrinsic tendency that stems from the chiral crystal structure (*5*,*6*). The second starts from the observation that, at very low supersaturation conditions, only nuclei of crystals that contain screw dislocations can grow further, as these dislocations create a more reactive crystal growth front (*1*, *12*-*17*). Such screw-dislocation-mediated growth yields helical shapes and has in the past been considered as a formation mechanism for twisted nanowires (*1*,*12*-*17*). It has not been considered, however, as a formation pathway for distinct chiral polyhedral shapes of crystals.

Differentiating between these two mechanisms is difficult, but the advent of controlled colloidal synthesis has allowed for studies of nanocrystals that have chiral crystal structures and form both

chiral and achiral shapes (*7-9*). Such nanostructures represent an embryonic stage in crystal growth and serve as convenient model systems to explore mechanisms of chiral shape formation (*7,9,18,19*). Previous studies concluded that chiral ligands are the cause for chiral shape formation. However, they did not explain why in many of these cases achiral shapes also formed in the presence of chiral ligands, and did not address other observations of chiral shape formation in the absence of chiral ligands (*1-6*).

Our system consists of tellurium nanocrystals with chiral shapes that are a few hundred nanometers in size (*7*). Tellurium crystallizes in one of the two enantiomorphous chiral space groups $P3_121$ or $P3_221$ (*7*). Growth of our nanocrystals involves reduction of tellurium dioxide in the presence of chiral thiolated penicillamine ligands and hydrazine that serves as a reducing agent, continuously supplying tellurium monomers for growth. Shapes of varying thickness were formed by blocking lateral growth at different stages of the reaction using sodium dodecyl sulfate (SDS). When added early in the reaction, thin twisted nanorods formed (Fig 1A and S1), and when added at a later stage, thick trigonal bipyramids formed (Fig. 1B and S1) . We characterized the bipyramidal nanoparticles using scanning transmission electron microscopy (STEM) tomography and scanning electron microscopy (SEM), thereby resolving the 3D chiral morphology. Figure 1C and movie S1 present 3D renderings of a representative bipyramid as viewed along the $[\bar{1}2\bar{1}0]$ direction. Several facets can be seen with smoothing due to the tomographic reconstruction process. SEM is highly sensitive to edges, and we used the tomography reconstructions of several NPs to better interpret SEM images of the sharply faceted structure. Figs. 1D-F and S2 show nanocrystals at the same orientation as in 1C , and Fig. 1G shows the bottom view, giving a sense of the overall shape. The trigonal symmetry is observed along the nanoparticle's long axis ($[000\bar{1}]$ direction) in Figs 1H and 1I using a TEM projection

and STEM tomography, respectively. This polyhedron possesses a D_3 point symmetry. STEM tomography and SEM images show that these nanoparticles present a distinct structure of flat facets with a chiral arrangement similar to chiral habits discussed in macroscopic crystals (*2*,*3*,*5*,*6*). We assigned left (M) and right (P)- handedness nomenclature to the shapes using a convention that follows reference (*9*). In this approach, the 3D shape can be thought of as a set of 2D slices stacked, and gradually rotating along the long axis ($[0001]$. Clockwise rotation is correlated with right-handedness and counter-clockwise with left handedness (Fig. S3). Further, the arrangement of two small facets in the center allows identifying the handedness, as it is mirrored in crystals of opposite chirality. These facets can be identified from the relative directions identified in Fig. 1H, and their indexing depends on which mirror image of the crystal is observed (see also Fig. 2). In right (P)- handed particles, these are the $(0\bar{1}10)$ and $(1\bar{1}00)$ facets colored pink and green, respectively (inset to Figs 1D-I). In left (M)- handed particles, these are the $(1\bar{1}00)$ and $(10\bar{1}0)$ colored green and orange, respectively. Extra facets on the sides (Fig. S4) are harder to assign but might be equivalent to those required in bulk chiral habits to lower shape symmetry, as in the case of quartz's s and x faces (5).

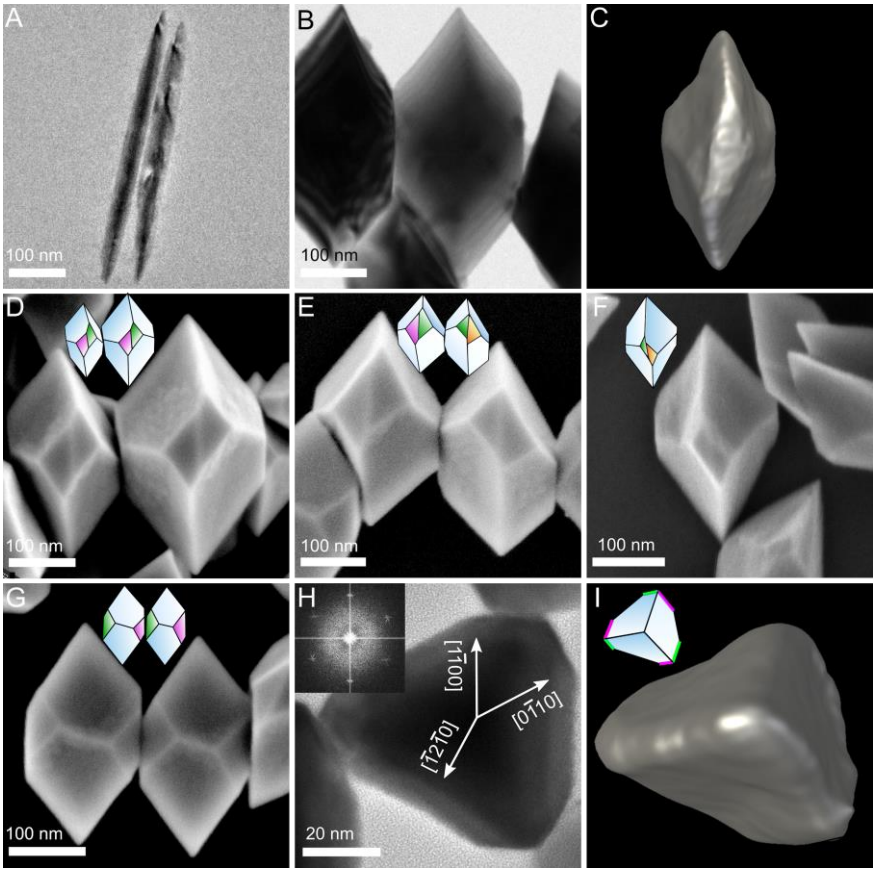

Fig. 1: Model system of morphologically chiral nanocrystals.

TEM images of (A) thin rods, and (B) fully formed bipyramids. (C) A surface rendering of a STEM tomogram of a bipyramid observed along the $[\bar{1}2\bar{1}0]$ direction. (D-F) SEM images of (D) a pair of right (P)-bipyramids, (E) a right (P)- and a left (M)- bipyramid, and (F) a single left (M)-bipyramid all observed along the $[\bar{1}2\bar{1}0]$ direction for P and $[1\bar{2}10]$ for M (G) A pair of right (P) bipyramids observed along the $[1\bar{2}10]$ direction. (H) A TEM image of a bipyramid observed along the $[000\bar{1}]$ direction, with its corresponding FFT. (I) A view along the $[000\bar{1}]$ direction of the tomogram in 1C. The pair of facets used to assign handedness are marked pink, green and orange on smaller inset models in D-G and I.

When the nanoparticles are prepared in the presence of one mirror image of the chiral ligand penicillamine, a large excess of one mirror image is formed as measured by circular dichroism (CD, Fig. S5). (*7-9*). CD does not allow quantifying the exact populations of mirror images; therefore, we used large-scale, automated SEM imaging and manual identification to distinguish the two forms from a large population of NPs (close to 300 in each sample).

In Fig. 2A, the distribution of both forms in samples made with pure D- and pure L-ligands is presented as a function of their length. In both samples, one mirror image formed in large excess (85%) but not 100%.The less-abundant particles are smaller in size, which indicates that chiral ligands affect the rates of both nucleation (affecting the population) and continuous growth (affecting the final size).

Next, we correlated the shape handedness with that of the crystal structure. For this purpose, aberration-corrected high angle annular dark field (HAADF-) STEM imaging at two stage tilts was performed. Fig. 2B presents low- and high-resolution HAADF-STEM images and an atomistic model viewed along the $1\bar{2}10$ tellurium nanocrystal direction. A single 2D STEM image, even though might appear to show chirality, does not decisively infer 3D handedness. Due to the projection nature of STEM, looking at the same particle from the opposite direction (corresponding to a 180 degree tilt) will reverse the sense of 2D handedness, and a single image is insufficient to tell which side the bipyramid is viewed. To solve this problem, we acquired a focal series as explained in the SI and Fig. S6,which allows us to assign left (M)- handedness to the particle observed in Fig. 2B. The same particle was then imaged at the $[1\bar{1}00]$ zone axis. The low-and high-resolution STEM images at the new orientation, and a model, are presented in Fig. 2C. Dong and Ma recently demonstrated that atomic-resolution images at these two tilts are sufficient to resolve the handedness of the crystal structure (*20*). Fig. 2C fits the model for the

$P3_221$ space group (left-handed tellurium helices), and will not fit the $P3_121$ space group (right-handed tellurium helices), which at these tilt conditions will exhibit a mirror arrangement of atoms. A detailed comparison and description of the space groups along these two directions is presented in Fig. S7. In the same way, it is determined that the particle observed along the $[\bar{1}2\bar{1}0]$ direction in Fig. 2D and $[\bar{1}100]$ in Fig. 2E, is a right (P)-handed particle with a crystal structure belonging to the $P3_121$ space group.

Both particles are from the sample depicted in the right panel of Fig. 2A, where right (P)-handed nanocrystals are more common. Using this method, we measured seven right (P)-handed particles and two left (M)- handed particles and found that P shapes always had the $P3_121$ space group, whereas M shapes had the $P3_221$ space group.

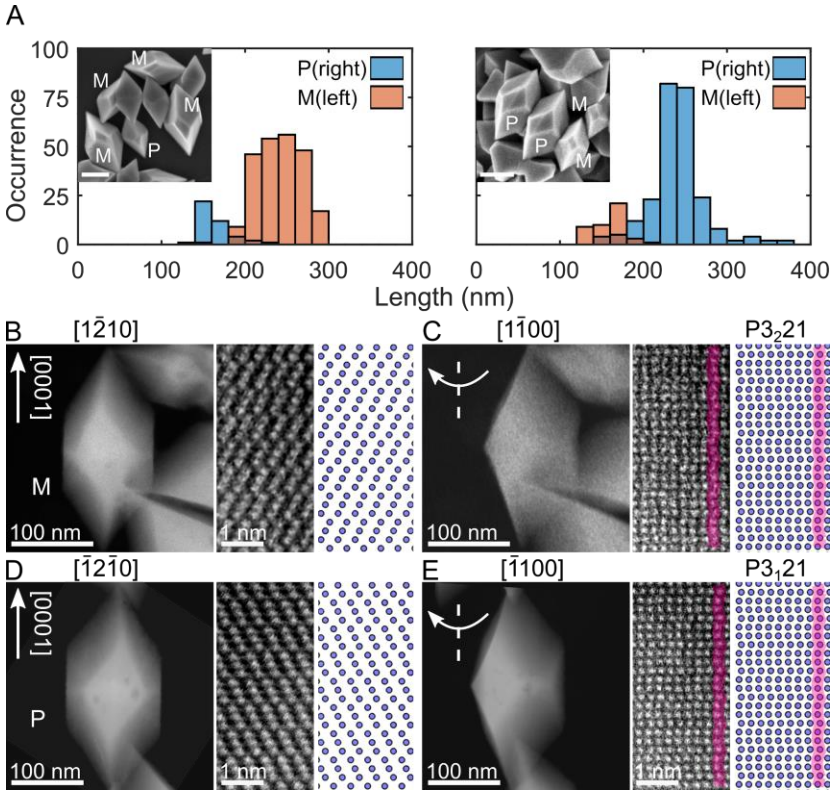

Fig. 2: Determination of crystal structure and shape handedness.

(A) Distribution of bipyramid handedness when using only L- and D- penicillamine ligand in the reaction (left and right, respectively). Orange and blue columns represent left- and right- handed particles, respectively. Bottom parts of columns that appear darker brown are where orange and blue overlap. In the insets, SEM images used for statistics show the existence of both mirror images (scale bars are 100 nm). (B,C) Low- (left) and high-resolution (middle) HAADF-STEM images and a corresponding atomistic model (right panel)of the (B) $[1\bar{2}10]$and (C) the $[1\bar{1}00]$ zone axes. Shape and crystal structure handedness was characterized as Mand $P3_221$ space group, respectively. Red curved lines highlight atom columns to compare between the experiment and model.. (D,E) A P-shaped nanocrystal observed along the (D) $[\bar{1}2\bar{1}0]$ and (E) $[\bar{1}100]$ directions. The crystal structure can be assigned to the $P3_121$ space group.

These results seem to imply that the chain of chirality transfer starts with the ligands directing the handedness of the crystal structure formation (but not with a 100% enantiomeric excess, and in turn, the crystal structure handedness determines that of the shape. However, as shown in Fig. 3, even though chiral ligands strongly affect the relative abundance of mirror images, they are neither necessary, nor sufficient for the formation of chiral shapes. The reaction was conducted with achiral mercaptopropionic acid as the thiolated ligand, under similar conditions, and the nanoparticles still formed a chiral shape similar to the ones formed with penicillamine (Figs. 3A, 3Band movie S2). This sample exhibited no CD signal, indicating that an equal mixture of left- and right-handed nanocrystals formed. These results indicate that chiral ligands only serve to bias the synthesis in favor of one mirror image, but do not cause chiral shape formation. This proves that past models of arrested growth by chiral additives (*2,9-11*) do not sufficiently describe the observations made here.

Next, we examined the other prominent mechanism that can lead to morphological chirality, screw-dislocation-mediated growth accompanied by "Eshelby twisting" of the crystal structure (*1,12-17*). Even though this mechanism is established as a source of shape chirality from twisting (*1,12-17*), we tested whether it also leads to the formation of the chiral polyhedrons. Classical crystal growth theory predicts that screw-dislocation-mediated growth is dominant at low monomer supersaturations (*12-16*). We therefore expected that if screw dislocations were involved, higher tellurium dioxide reduction rates should produce achiral shapes. Achiral morphologies indeed formed in these conditions, even in the presence of chiral ligands at the same concentration as in the reactions that yielded chiral shapes (Fig 3C, 3D and movie S3). Figs. 3E-H show the transition from chiral (3E-G) to achiral (3H) shape formation as the rate of reduction, which sets supersaturation conditions, is increased. Other than the rate of reduction, all synthetic conditions are identical between these samples. The TEM images show that particles in Figs. 3E-G have the chiral shape seen in Fig. 1B, and the ones in 3H have the achiral shape seen in Figs. 3C,D. The CD response shown below each TEM image (expected to be present only for chiral shapes) (*7*)is absent for the particles in Fig. 3H. This observation correlates with the model predicting a transition from screw-dislocation-driven growth to layer-by-layer growth (*12-16*).

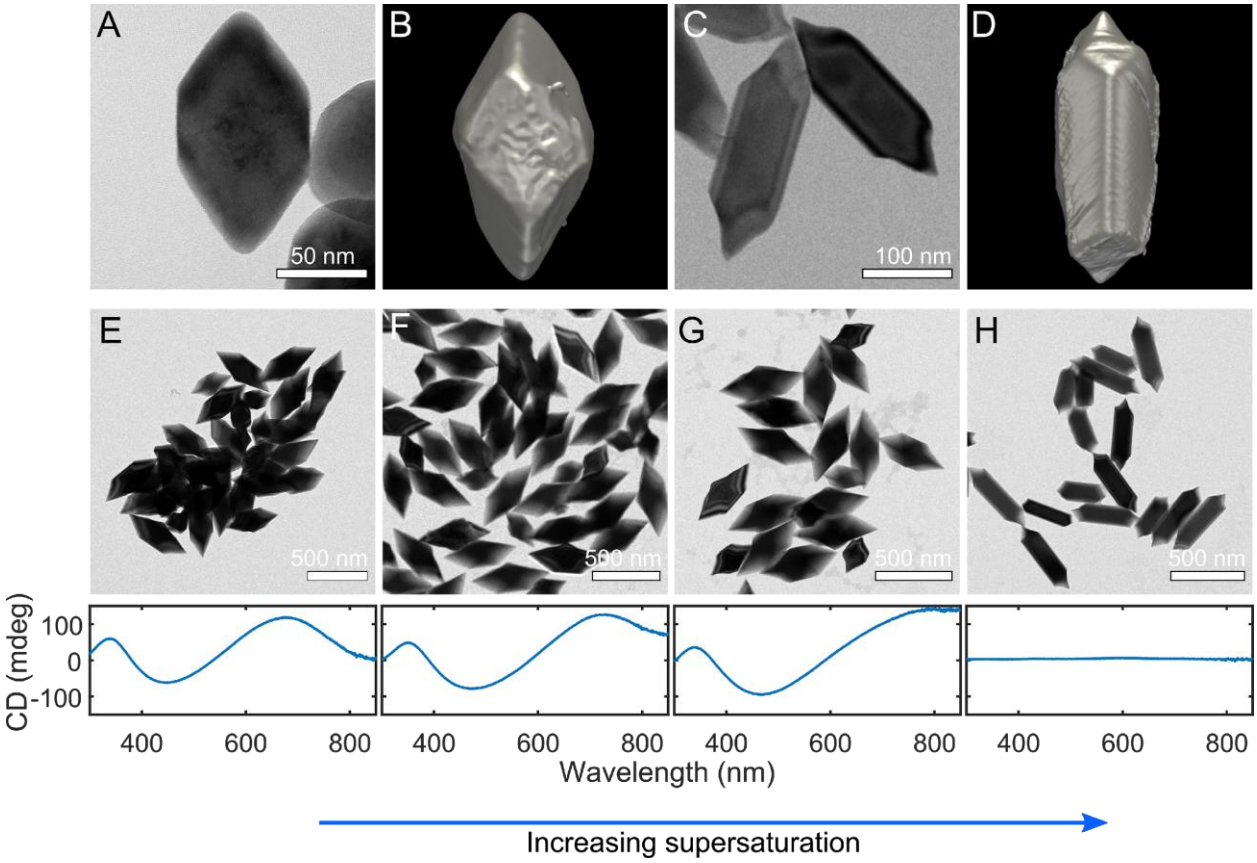

Figure 3: Chiral ligands are neither necessary nor sufficient for chiral shape formation. (A) A TEM image, and (B) a STEM tomogram of chiral bipyramids grown with achiral mercaptopropionic acid ligands. (C) A TEM image, and (D) a STEM tomogram of achiral particles grown with chiral penicillamine ligands. (E-H) TEM images with the corresponding CD spectra below, of particles grown with (E) 1 ml, (F) 2 ml, (G) 4 ml and (H) 6 ml of hydrazine. The transition from chiral to achiral morphology is observed between G and H.

We support these results, which strongly imply the involvement of screw dislocations in the growth process, with structural characterization. Aberration-corrected HAADF-STEM imaging allowed directly observing atomic displacements induced by the dislocation, but two cases must be considered. First, a single screw dislocation line passes through the core of the nanorod (*12*-

17). Second, as commonly observed in tellurium (*21*,*22*) and other systems (*22*,*23*), he screw dislocation dissociates into partials, thereby lowering the crystal's overall energy. In the case of tellurium, a single screw dislocation with a Burgers vector $b = [0001]$ can dissociate into three partials with $b = \frac{1}{3}[0001]$ (*20*,*21*). In Fig. 4A, a HAADF-STEM image of a thin rod observed along the $[1\bar{2}10]$ direction is presented. In Fig. 4B, the region marked by a cyan frame in Fig 4A is magnified and compared with a model of a dissociated screw (see SI methods and Fig. S8). A discontinuity in the rows of atomic columns is observed across the dislocation line. This is a signature of the a dissociated screw and is not observed in a crystal with a non-dissociated screw (Fig. S8). Images of another nanoparticle and direction also show the atomic column displacements of the line defect (Fig. S9).

Another indication of screw dislocations is the Eshelby twisting of the lattice (12-17) which we measured using four-dimensional STEM (4D-STEM) (24), a technique that allows extracting local twisting with high spatial resolution (methods and Fig. S10). In brief, a measurement of 2D electron diffraction patterns is acquired at a 2D set of scanning positionsand Laue circle fitting for each scan positionmaps the local lattice orientation. relative to the [0001] axis (Figure 4C). Representative diffraction patterns with red fit lines from three beam positions are presented. Twisting along the C-axis of 0.02deg/nm is measured similar to other measurements of Eshelby twisting (*12-14*). Existence of this twist further reduces the possibility that chirality of the shape originates from differential growth rates of facets induced by chiral ligands or by the chiral crystal structure, as this would not be accompanied by lattice twisting.

Screw dislocations can also lead to void formation due to the strain energy associated with the dislocation exceeding the surface energy required to form an inner surface (*14*). In Fig. 4D and 4E representative HAADF-STEM images of rods and bipyramids, respectively, show these voids

as dark regions. STEM tomography shows voids inside the nanoparticle (Fig. S11.). As expected, voids were not found in achiral shapes (Fig S. 12), but were found in chiral shapes grown in the absence of chiral ligands (Fig. S13).

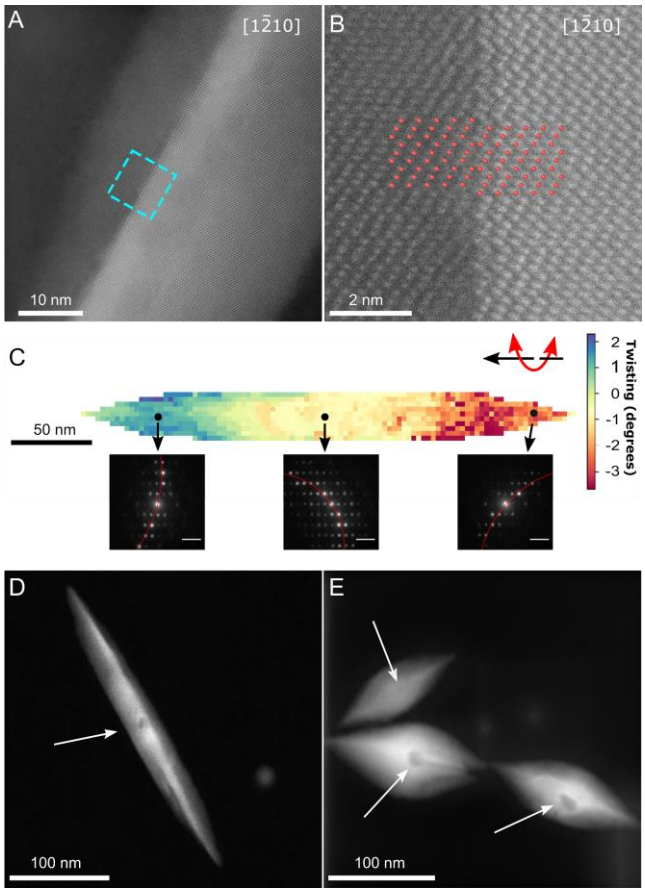

Figure 4: Structural evidence of screw dislocations.

(A) An atomic resolution HAADF-STEM image of the center of a nanorod observed along the [1$\bar{2}$10] direction. (B) The enlarged region marked by a cyan frame in 3A overlaid with a model for a dissociated dislocation (red dots). (C) Map of twist around the C-axis extracted from 4D-STEM measurements. Electron diffraction patterns from different positions are overlaid with fits

to a Laue circle (red lines). (D,E) HAADF-STEM images of (D) a nanorod and (E) bipyramids with voids (white arrows).

Combined, our results strongly suggest a chain of chirality transfer from crystal structure to shape that is not a result of the chiral crystal structure or chiral ligands. Instead, chiral shapes form when grown in sufficiently low supersaturation such that they are the result of screw-dislocation-mediated growth. The fact that the handedness of the shape seems to be dictated by that of the crystal structure is probably a result of screw dislocations of opposite handedness being favored in crystal structures of opposite handedness (*25*,*26*). In this way, screw dislocations also mediate correlation of handedness between the two hierarchies. Even though chiral ligands do not give rise to chiral shapes in our system, they can bias the population of both mirror images, leading to an abundance of one mirror image over the other, as well as a difference in average size . This suggests chiral ligands unevenly affect opposite mirror images of chiral crystals in both the nucleation and growth stages. Although screw-dislocation-mediated growth has been studied in relation to twisting, it has rarely been considered as the source of habits of single crystals that present a chiral arrangement of facets. It is not surprising that such a mechanism has been overlooked in bulk crystals that present chiral non-twisted habits, as the signature of these dislocations in growth would have been very hard to identify.

References and Notes:

1. A. G. Shtukenberg, Y. O. Punin, A. Gujral, B. Kahr, Growth actuated bending and twisting of single crystals. *Angew. Chem. Int. Ed.* **53**, 672-699 (2014).
2. L. Addadi, M. Geva, Molecular recognition at the interface between crystals and biology: generation, manifestation and detection of chirality at crystal surfaces. *Cryst. Eng. Comm.* **5**, 140-146 (2003).
3. L. Pasteur, Sur les relations qui peuvent exister entre la forme cristalline, la composition chimique et le sens de la polarisation rotatoire. *Ann. Chim. Phys.* **24**, 442–459 (1848)
4. J. Gal, The discovery of biological enantioselectivity: Louis Pasteur and the fermentation of tartaric acid, 1857- A review and analysis 150 Yr later. *Chirality* **20**, 5-19 (2008).
5. R. M. Hazen, D. S. Sholl, Chiral selection on inorganic crystalline surfaces. *Nat. Mater.* **2**, 367–374 (2003).
6. K.- H. Ernst, Molecular chirality in surface science. *Surf. Sci.* **613**, 1-5 (2013).
7. A. Ben-Moshe, S. G. Wolf, M. Bar-Sadan, L. Houben, Z. Fan, A. O. Govorov, G. Markovich, Enantioselective control of lattice and shape chirality in inorganic nanostructures using chiral biomolecules. *Nat. Commun.* **5**, 4302 (2014)
8. A. Ben-Moshe, A. O. Govorov, G. Markovich, Enantioselective synthesis of intrinsically chiral mercury sulfide nanocrystals. *Angew. Chem. Int. Ed.* **52**, 1275-1279 (2013).
9. P.-P. Wang, S.- J. Yu, A. O. Govorov, M. Ouyang, Cooperative expression of atomic chirality in inorganic nanostructures. *Nat. Commun.* **8**, 14312 (2017).
10. I. Weissbuch, L. Addadi, M. Lahav, L. Leiserowitz, Molecular recognition at crystal interfaces. *Science* **253** 637-645 (1991).
11. C. A. Orme, A. Noy, A. Wierzbicki, M. T. McBride, M. Grantham, H. H. Teng, P. M. Dove, J. J. DeYoreo, Formation of chiral morphologies through selective binding of amino acids to calcite surface steps. *Nature* **411**, 775–779 (2001).
12. M. J. Bierman, Y. K. Albert Lau, A. V. Kvit, A. L. Schmitt, S. Jin, Dislocation-driven nanowire growth and Eshelby twist. *Science* **320**, 1060-1063 (2008).
13. J. Zhu, H. Peng, A. F. Marshall,D. M. Barnett, W. D. Nix, Y. Cui, Formation of chiral branched nanowires by the Eshelby twist. *Nat. Nanotech.* **3**, 477-481 (2008).
14. S. A. Morin, M. J. Bierman, J. Tong, S. Jin Mechanism and kinetics of spontaneous nanotube growth driven by screw dislocations. *Science* **328**, 476-480 (2010).
15. F. Meng, S. A. Morin, A. Faurticaux, S. Jin, Screw dislocation driven growth of nanomaterials. *Acc. Chem. Res.* **46**, 1616–1626 (2013).
16. Y. Liu, J. Wang, S. Kim, H. Sun, F. Yang, Z. Fang, N. Tamura, R. Zhang, X. Song, J. Wen, B. Z. Xu, M. Wang, S. Lin, Q. Yu, K. B. Tom, Y. Deng, J. Turner, E. Chan, D. Jin, R. O. Ritchie, A. M. Minor, D. C. Chrzan, M. C. Scott, J. Yao, Helical van der Waals crystals with discretized Esehlby twist. *Nature* **570**, 358-362 (2019).
17. L. H. G. Tizei, A.J. Craven, L. F. Zagonel, M. Tencé, O. Stéphan, T. Chiaramonte, M. A. Cotta, D. Ugarte, Enhanced Eshelby twist on thin wurtzite InP nanowires and measurement of local crystal rotation. *Phys. Rev. Lett.* **107**, 195503 (2011).
18. A. Ben-Moshe, B. M. Maoz, A. O. Govorov, G. Markovich, Chirality and chiroptical effects in inorganic nanocrystal systems with plasmon and exciton resonances. *Chem. Soc. Rev.* **42**, 7028-7041 (2013).
19. J. Yeom, B. Yeom, H. Chan, K. W. Smith, S. Dominguez-Medina, J. H. Bahng, G. Zhao, W.-S. Chang, S.-J. Chang, A. Chuvilin, D. Melnikau, A. L. Rogach, P. Zhang, Stephan

Link, P. Král, N. A. Kotov, Chiral templating of self-assembling nanostructures by circularly polarized light. *Nat. Mater.* **14**, 66-72 (2015).
20. Z. Dong, Y. Ma Atomic-level handedness determination of chiral crystals using aberration-corrected scanning transmission electron microscopy. *Nat. Commun.* **11**, 1588 (2020).
21. J. Di Persio, J. C. Doukhan, G. Saada, Les dislocations dans la structure du tellure. *J. Phys. France* **28**, 661-666 (1967).
22. B. Escaig, Dissociation and mechanical properties. Dislocation splitting and the plastic glide process in crystals. *J. Phys. colloques* **35**, C7-151 - C7-166 (1974).
23. S. Ismail-Beigi, T. A. Arias, Ab Initio study of screw dislocations in Mo and Ta: A new picture of plasticity in bcc transition metals. *Phys. Rev. Lett.* **84**, 1499-1502 (2000).
24. C. Ophus, Four-Dimensional scanning transmission electron microscopy (4D-STEM): From scanning nanodiffraction to ptychography and beyond *Micros. Microanal. **25**, 563-582* (2019).
25. A. G. Shtukenberg, L. N. Poloni, Z. Zhu, Z. An, M. Bhandari, P. Song, A. L. Rohl, B. Kahr, M. D. Ward, Dislocation-actuated growth and inhibition of hexagonal L-cystine crystallization at the molecular level. *Cryst. Growth Des.* **15**, 921-934 (2015).
26. B. Sung, A. de la Cotte, E. Grelet, Chirality-controlled crystallization via screw dislocations. *Nat. Commun.* **9**, 1405 (2018).
27. C.-Y. Wen, X. J. Guo, J. H. Huang, H. C. Shih, Determination of the three-dimensional crystallographic misorientation in heterostructures by selected area diffraction (SAD) in cross-sectional TEM. *Journal of Crystal Growth* **213**, 150–156 (2000).
28. N, Chernov, C, Lesort, Least squares fitting of circles. *Journal of Mathematical Imaging and Vision* **23 (3)**, 239–252 (2005).
29. J. Jansen, M. T. Otten, H. W. Zandbergen, Towards automatic alignment of a crystalline sample in an electron microscope along a zone axis. *Ultramicroscopy* **125**, 59–65 (2013).
30. G.-H. Kim, H.-S. Kim, D.-W. Kum, Simple procedure for phase identification using convergent beam electron diffraction patterns. *Microscopy Research and Technique* **33 (6)**, 510–515 (1996).
31. C. Gammer, V. Burak Ozdol, C. H. Liebscher, A. M. Minor, Diffraction contrast imaging using virtual apertures. *Ultramicroscopy* **155**, 1–10 (2015).
32. E. F. Rauch, M. Véron, Virtual dark-field images reconstructed from electron diffraction patterns. *The European Physical Journal Applied Physics* **66 (1)**, 10701 (2014).
33. K. Persson, Materials data on Te (SG:152) by Materials Project. (2016). doi:10.17188/1193780
34. P. M. Anderson, J. P. Hirth, J. Lothe, Theory of dislocations. Cambridge University Press, (2017).
35. A. N. Stroh, Dislocations and cracks in anisotropic elasticity. *J. Theor. Exp. Appl. Phys.* **330**, 625–646 (1958).
36. A. Stukowski, Visualization and analysis of atomistic simulation data with OVITO–the Open Visualization Tool. *Model. Simul. Mater. Sci. Eng.* **18**, 015012 (2010).
37. K. Momma, F. Izumi, VESTA 3 for three-dimensional visualization of crystal, volumetric and morphology data. *J. Appl. Crystallogr.*, **44**, 1272-1276 (2011).

Acknowledgments: We are very grateful to Dr. Min Gee Cho for her help with HR imaging, to Dr. Karen Bustillo for help with 4D-STEM data collection, Chengyu Song for assistance in STEM imaging, and to Charlotte Nixon and Prof. Susan Marqusee for graciously allowing us to use their group's CD spectrometer and supporting us in the process. A.B.M is grateful to Dr. Ayelet Teitelboim for useful discussions and her support. We are very grateful to Prof. Yanhang Ma for useful discussion regarding determination of crystal structure handedness in STEM.
Funding: This work was primarily supported by the U.S. Department of Energy, Office of Science, Office of Basic Energy Sciences, Materials Sciences and Engineering Division, under Contract No. DE-AC02-05-CH11231 within the Characterization of Functional Nanomachines Program (KC1203). Work at the Molecular Foundry, Lawrence Berkeley National Laboratory, was supported by the U.S. Department of Energy under contract no. DE-AC02-05CH11231. J. W. acknowledges support from the U.S. Department of Energy, Office of Science, Office of Workforce Development for Teachers and Scientists (WDTS) under the Science Undergraduate Laboratory Internship (SULI) program. F.N was supported by the Miller Research Institute. A.B.M acknowledges support from a Fulbright fellowship. A.d.S acknowledges funding from the Brazilian National Council of Technological and Scientific Development (CNPq). A.A. and M. A. acknowledge support for the computational modeling from a fellowship through the National Science Foundation Graduate Research Fellowship Program (Grant No. DGE 1752814), and the U.S. Department of Energy, Office of Science, Office of Basic Energy Sciences, Materials Sciences and Engineering Division, under Contract No. DE-AC02-05-CH11231 within the Damage-Tolerance in Structural Materials (KC 13) program, respectively.
Author contributions: A.B.-M. and A.P.A conceived of the idea for the project. A.B.-M. performed synthesis of nanocrystals, TEM characterizations and CD measurements. A.d.S. performed data acquisition and analysis for STEM tomography supervised by P.E. 4D-STEM data was collected by A.d.S, and analyzed by A.d.S and P. H., supervised by W.T. and P.E. A.M. acquired large scale SEM scans and HR-SEM, and the data was analyzed by A.M., J.W. and A.B.-M. F.N. performed additional SEM characterizations. P.E. performed HR-STEM imaging. A.M.M., W.T., and P.E. supervised all the electron microscopy work. A.A. developed the continuum elasticity models supervised by M.A. A.B.-M. and A.P.A. wrote the manuscript, with critical contributions and edits from all authors. A.P.A directed the project.
Competing interests: The authors declare no competing interests. **Data and materials availability:** All data is available in the main text or the supplementary materials.

Supplementary Materials:

Materials and Methods

Figures S1-S13

Movies S1-S3

References (*27-37*)